Diagnostics of sprays with wide droplet-size distribution by novel interferometric laser imaging technique

T.Kawaguchi[1], K.Matsuura[2], K.Ueyama[2] and M.Maeda[1]

1. Keio University, Hiyoshi 3-14-1, Kohoku Yokohama 223-8522 Japan.
2. KANOMAX Japan Incorporated, Shimizu 2-1, Suita Osaka 565-0805 Japan.

For understanding the transient spray, not only the size and velocity distribution of droplets but those simultaneous properties of individual droplets are required to understand the unsteady behavior of flow fields. The improved interferometric imaging technique has been developed by the authors that can measure the planar or volumetric distribution of diameter and velocity vector of droplets instantaneously. The accurate diameter determination by the optical compression and subpixel frequency estimation by a Gaussian interpolation technique enables the accurate determination of the droplet correspondence between two successive images and consequently the velocity vectors of each droplet can be measured even from the image of denser spray. The direct digital acquisition of images and fully automated image processing software provide the high quality data, up to six hundred droplets in a frozen image of 10mm$\times$10mm. Further, the time-series properties of flow at various periods after the start of injection are obtained by the phase-averaged flow resume. The results showed the significant difference of droplet behavior depending on the group of diameters in the transient spray.

1 Introduction

The analysis of such dispersed two phase flow as spray needs information on size and velocity vector field of particles. Phase Doppler Anemometry (PDA), which is an extension of Laser Doppler Anemometry (LDA), can provide the size and velocity vector of a single transparent particle within the small measurement volume more or less at a point.[1] PDA has been applied to various kinds of flow field to obtain the accurate size and velocity by many investigators.[2–4] Some reports concluded that there are undesired effects on the estimation of mass flux of droplets due to the determination of the effective measuring area, *i.e.* particle size-dependent detection area, trajectory ambiguity, slit effect and the Gaussian beam effect. Point measurement, however, provides little information on the spatial structure of the flow field, the distribution of particle size and velocity, and the dynamic interaction among them.

Interferometric laser imaging for droplet sizing (ILIDS) is a technique that can provide the instantaneous size and spatial distribution of droplets. The method observes the spatial pattern of laser light scattered by a transparent spherical droplet. The characteristic interferogram is generated by the interference of reflection and refraction components from an incident single light sheet on the droplets. The fringe spacing of the ILIDS interferogram is correlated with individual particle sizes. König *et al* [5] investigated the relation between droplet diameter and the fringe count or the number of fringes by geometrical optics. The technique was further improved by Glover *et al* ,[6] Skippon and Takagi,[7] who analyzed the features of the scattered light around the forward scatter regions and applied the technique to spatially sparse sprays. Although the technique successfully obtained the droplet size from a single image in a dilute

part of spray, the much denser part of spray remained unmeasurable even though it is quite important to identify the structure of these flow fields. Conventional ILIDS, which observes parallel fringes in circular image on a film, has difficulties in evaluating the fringe spacing accurately due to overlapping of the circular image at high concentration.

The objective of the present study is to develop the simultaneous measurement technique of size and velocity vector of individual spherical particles in flow field. The paper describes an improvement to the interferometric laser imaging technique[8–11] with an automated measuring system by employing a high resolution digital CCD camera and high speed computing system. In order to make the system feasible to measure denser droplet fields, the anamorphic image acquisition optics was employed, which has different focal length along mutually perpendicular radii, to overcome image overlapping of the circular non-compressed interferogram. The enhancement of sizing accuracy enables the precise tracking of droplets between two images and consequently the velocity vectors could be determined in the spray flows with distributed size. The present technique has the following significant features for the measurement of sprays.

1. The technique improves the optical signal to noise ratio by integrating the circular image with fringes and the determination of the frequency, which is directly proportional to the droplet diameter by geometric optics, becomes accurate.
2. Distorted and/or irregular fringes that are caused by multiple scattering, or any other optical path changes, can be validated automatically since the distorted high frequency interferential pattern will disappear by spatial integration of the image.
3. The range of the measured diameter can be adjusted by changing the alignment of a pair of cylindrical lenses and the aperture size of the receiving optics.
4. By using direct digitization and a computer system, reliable determination of individual particle diameter is accomplished. The image processing procedure is simplified and less time-consuming.
5. From the captured data set, the spatial resolution of measured diameter and velocity can be optimized by adjusting and selecting the size of the probe area in the captured image.
6. The measured result provides the instantaneous distribution of droplet size, concentration and velocity. Moreover the size-dependent velocity vector field in the steady and even in the transient flow can be obtained.

2 Improved interferometric laser imaging technique

Light scattering pattern as shown in Figure 1 provides a lot of significant characteristics of particle. When a transparent spherical droplet in the flow field is illuminated by a laser source, the reflected and first order refracted light from the droplet are dominant in the wide angle forward scatter region around 30–80 degrees. The present technique will focus on the fine structure around the forward scattering region. On the focal image plane, not an external shape of droplet but a couple of glare points can be observed. Although the droplet diameter can be determined from the interval between the spots,[12] it is hard to know the glare points separation in an actual flow fields due to the lack of spatial resolution and the necessity of magnification of the receiving equipment. Outside the focal plane, the reflection and refraction spots become larger and the interference is observed in their overlapping region. The interferometric laser imaging technique provides the droplet diameter by relating this to the spacing of the fringes in the interference image.

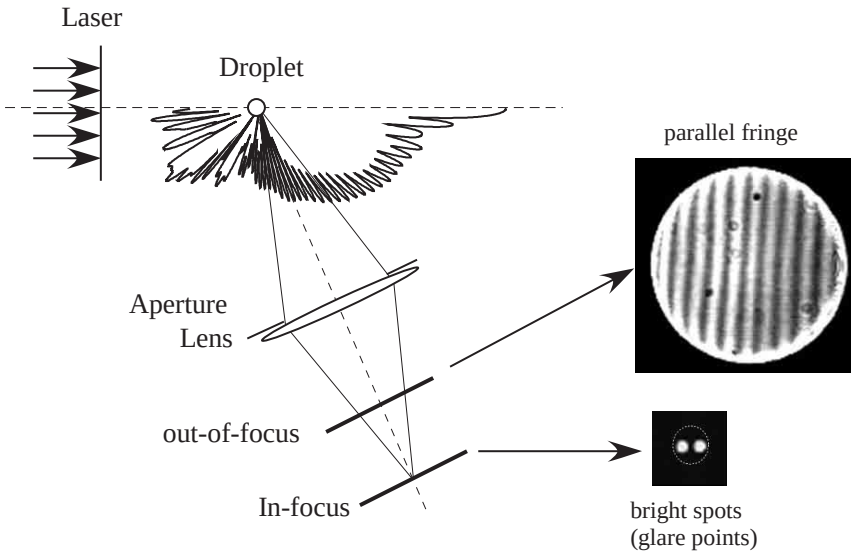

Figure 1: Scattered light intensity from a transparent spherical droplet illuminated by a laser light and in-focus and out-of-focused image of a droplet.

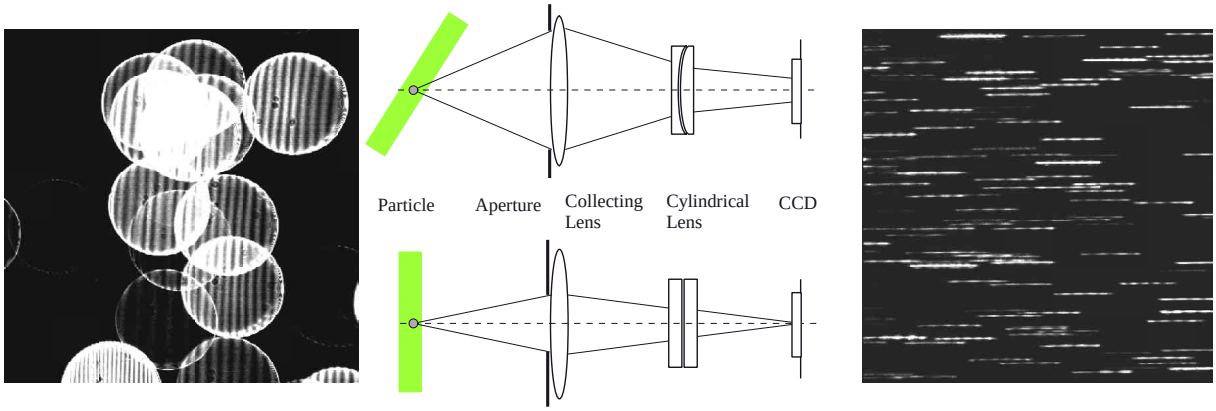

Figure 2: Details of the fringe squeezing optics and the example of a portion of the measured interferometric image ($4 \times 4\mathrm{mm}$). (left):Using the conventional ILIDS technique even 15 particles become difficult to measure in the specified area. (right):Using the optical partial compression technique, more than 100 particles can be identified in the frame.

In the original ILIDS techniques the fringes in the circular images are captured on the out-of-focus optical plane. Figure 2 illustrates the simplified schematic of the improved receiving optics and comparison of the captured images between conventional ILIDS technique (left) and improved technique (right) The imaging optics consisted of a rectangular aperture, a circular objective lens, a pair of cylindrical lenses and a CCD camera. A pair of cylindrical lenses located between the CCD camera and the objective lens generates horizontal out-of-focus images on a focus plane. The cylindrical lens can shift along the optical axis and it enables adjustment of the degree of horizontal defocusing. The radius of the circular images with different numbers of fringes in Figure 2 are the same since the image size is correlated with the collecting angle or the aperture size, *i.e.*, it is the number of fringes or fringe spacing that gives the droplet size.

The problem of the conventional technique is the difficulty in identifying individual images due to the overlapping of the circular interferogram in high particle concentration regions. By using this anamorphic optical system, which has different focal length along mutually perpendicular radii, the image overlapping can be drastically decreased and the vertical focusing of the interferometric images becomes clearer. Figure 2 demonstrates the significant improvement of the present method afforded by a partial compression technique. Moreover the image squeezing technique enhances the signal to noise ratio of the captured interferential image and can reject the signals with distorted or inclined fringes by wrong incident light automatically.

The present study also developed a computer aided automatic image processing method with the optimized software written in C/C++ and run on a personal computer. The software first identifies the individual linear fringe images and their location by scanning the captured image that is similar to Doppler burst signals by laser Doppler velocimeter. The concept of the signal processing methods to evaluate the fringe spacing is the same as FFT-based laser Doppler velocimeter or phase Doppler anemometry technique by which the frequency is calculated with an adjusted Gaussian fitting of the discrete Fourier power spectrum.[13,14] The interpolation technique reduces the bias error to less than 0.2% of the fundamental frequency.

3 Experiments and Results

A simplified depiction of the experimental apparatus is illustrated in Figure 3. The measurement equipment consisted of a high power laser light source, receiving optics, timing controller and personal computer. The optical and electronic devices for the present technique are basically the same equipment as for conventional particle image velocimetry or particle tracking velocimetry system. The laser source and CCD camera and fuel injector was operated by the single timing controller to capture the image at the specified time after start of injection of n-heptane. Injection and ambient pressure was set to 1.0MPa and 0.1MPa respectively. Injection interval was set to 100ms due to the maximum repetition frequency of optical system. The laser source was double-pulsed Nd:YAG laser at 532 nm in wavelength with the maximum output power of 120 mJ/pulse, maximum repetition frequency of 15 Hz. The duration time of the laser pulse was 3–5 ns. The thickness of the laser sheet at the test section was 0.5 mm. The laser light was circularly polarized to distinguish the interferometric signal from the background noise on the image. Projected images with fringes were captured by a high resolution digital CCD camera which acquired and transferred the progressive image sequence to the computer's memory directly. The CCD camera had 1008×1018 pixels, each pixel was a 10bit grayscale accuracy and the size of each pixel was $9\mu m\times9\mu m$. The viewing area of the receiving optics was $10mm\times10mm$. The distance of the objective lens and the test section was 180 mm, scattering was 70 degree that gives the maximum visibility of interference signal. The collecting angle was set to 10 degrees, which was calculated from the working distance op the receiver and the effective diameter of the objective lens. In the present experimental set-up, measurable diameter and velocity range was 2–150μm and ±100m/s for each velocity components, respectively. For the measurement of smaller or larger droplets, the measurable diameter range can be widely adjusted by the sophisticated technique in conjunction with the present compression technique.

Figure 4 is an example of the measured results in $z = 25$mm, 45mm of $r = 20$mm from the nozzle at $t = 4.2$ms after the start of injection. The white rectangle within the spray picture represents the viewing area of the receiving optics of $10mm\times10mm$. The result gives the instantaneous droplet locations, individual diameters and velocity vectors, and shows that the

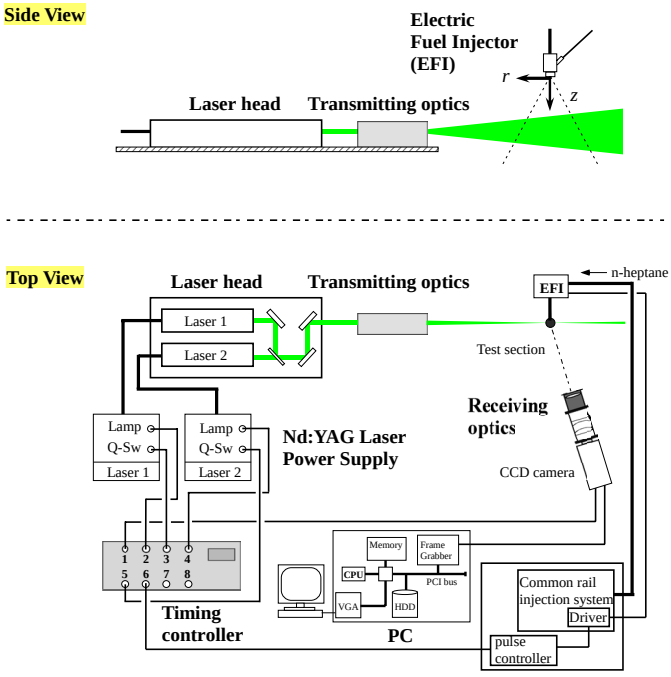

Figure 3: Fully synchronized image acquisition system for the transient spray system.

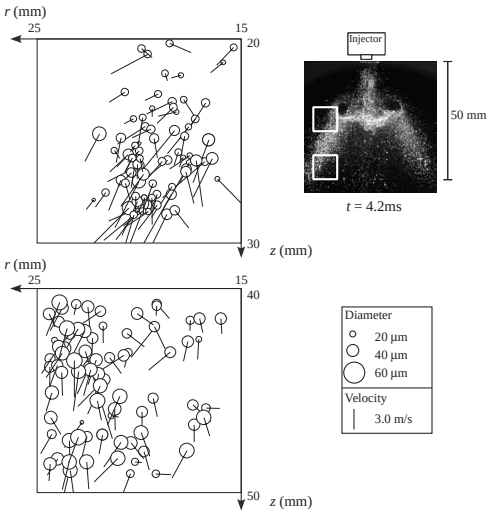

Figure 4: Examples of the measured result of instantaneous droplet size and velocity distribution from the single frozen image.

upper region contains the dense smaller particle below $z = 25$mm and the lower contains larger droplets at $r > 20$mm.

Figure 5 is the snapshots of the entire spray in 90mm $\times$ 90mm at t=2.5ms to 5.0ms in every 0.5ms after the start of injection. At the beginning of the injection, droplets were distributed in a triangular region from the fuel injector and characteristic transition of droplet distribution was appeared at t=3.0ms. Figure 6 shows the probability density function of the measured droplet diameter detected in the specified measurement region at t=3.0, 4.0 and 5.0ms. Measured location shown in the figure was 0–20mm in radial direction, 0–40mm in axial direction. At t=3.0ms, the size of measured droplet was widely distributed in the every location. In contrast, the distribution become sharpen and mean diameter at t=5.0ms has decreased especially in the vicinity of the injection nozzle.

Figure 7 is a comparison of the instantaneous spatial distribution of number count within the specified volume or concentration of smaller and larger droplet at t=2.5ms and 4.5ms. The width, height and thickness of the volume were 10mm, 10mm and 0.5mm respectively. In the Figure 7, the snapshot of the focused image of entire spray was also given to understand the brief structure of flow fields. The size of viewing area was 40mm$\times$60mm from the injection nozzle. The diameter range in this case was set to $d <$20µm and 20$< d <$30µm. The spatial distributions of concentration at t=2.5ms is not so different, particle is concentrated toward the injection angle and directly under the nozzle. At t=4.5ms larger droplet reached further downstream region rapidly due to the larger momentum of individual droplets in contrast with the entrained smaller droplets by the large scale vortex.

Figure 8 illustrates the size-dependent velocity vector maps in the magnified area at r=10mm,

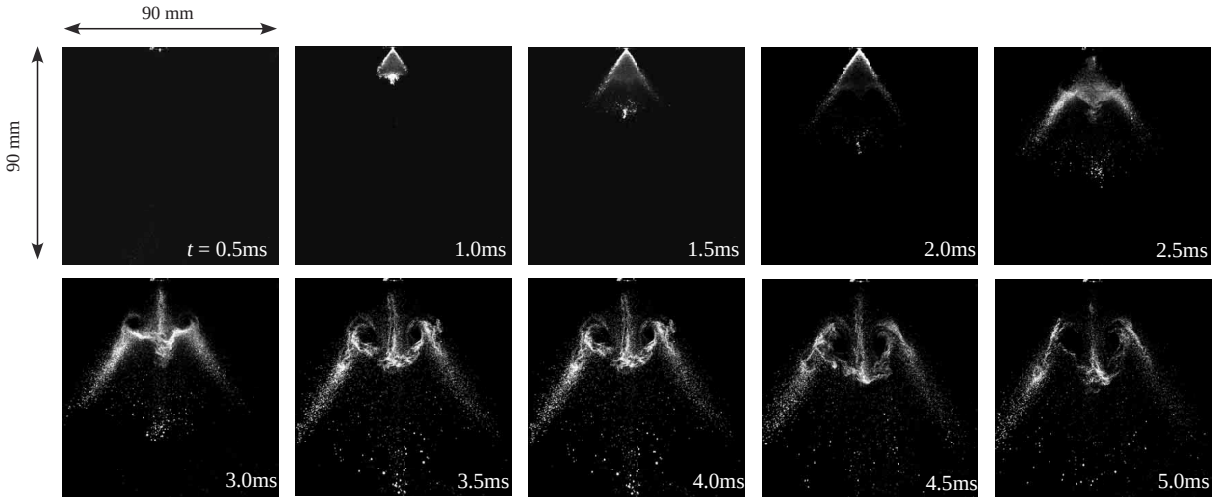

Figure 5: Snapshots of the spray from t=2.5ms to 5.0ms in every 0.5ms after the start of injection.

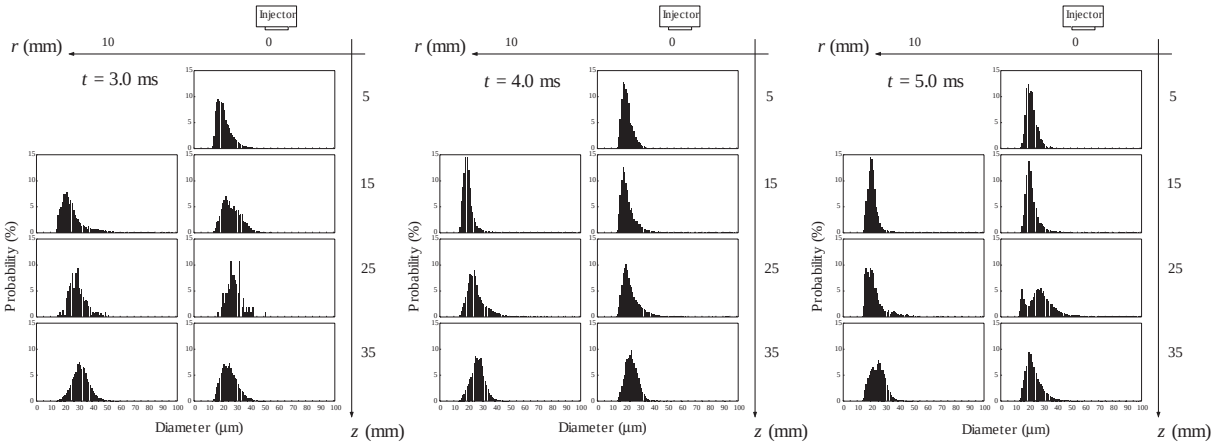

Figure 6: Probability density function of the droplet diameter at t=3.0ms to 5.0ms in every 1.0ms after the start of injection corresponding to Figure 5.

z=15mm and comparison between PIV and present technique. The probability density function of the droplet diameter at the corresponding area is also shown in Figure 8. By noting the diameter distribution, the diameter range was set to (a) d <20μm, (b) 20< d <30μm and (c) 30μm< d. Each vector was obtained by calculating the arithmetic mean velocity of the droplets within the 0.4×0.4mm subregion. The velocity of the smaller droplets (a) and (b), which contain the peak of the probability density function of diameter, shows the drastically change in velocity caused by the entrainment of spray. In contrast, the velocity distribution of the larger droplets (c) is higher and almost homogeneously directed downward. In the result, the velocity distribution obtained by PIV technique is similar to the velocity vector map of larger droplet obtained by the present technique. The comparison of the velocity maps demonstrate the remarkable difference of the absolute velocity and flow direction in the specified area where the characteristic hollow structure of the droplet concentration appears. Although the vector maps have an appearance similar to that of PIV results, the maps obtained by the present technique show the diameter-

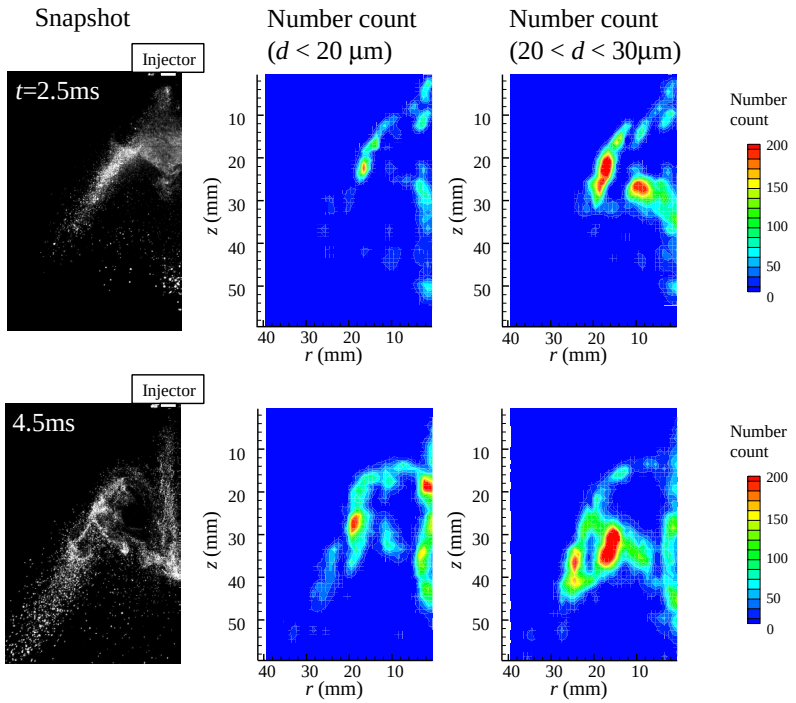

Figure 7: Instantaneus distribution of droplet number count within measurement area and corresponding spray image.

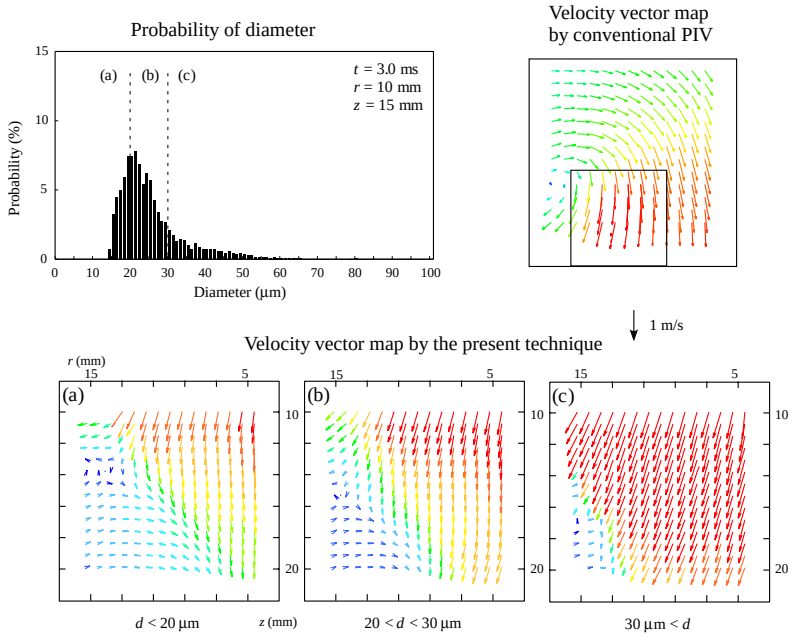

Figure 8: Probability density function of the droplet diameter and comparison of velocity vector maps by conventional PIV and by spatially averaged velocity of the present techniques at the exactly same observation area in flow. The velocity vector map by the present technique was classified by the diameter.

dependent velocity from the same domain separately and show that the velocity of the smaller droplets is comparatively slow throughout the given area in contrast with the high velocity of the larger droplets.

Conclusions

A novel interferometric laser imaging technique for droplet sizing has been developed. The image compression technique can enhance the optical signal to noise ratio of the captured interferential image and can reject the signals with distorted or inclined fringes by wrong incident light automatically. The significant advantage of the present technique is that the precise diameter determination of individual droplets enables the correct identification of the particle in two images which permits particle tracking algorithm to be used. The technique was applied to the measurement of transient spray of n-heptane and provided a temporal and spatial distribution of particle diameter, concentration and velocity vector field of droplet. The comparison of the size-dependent velocity vector maps demonstrates the remarkable difference of the velocity fields due to the droplet diameter even in the same observation area.

Acknowledgment

The present work was supported by a Grant-Aid of the Japanese Ministry of Education, Science and Culture (Grant No. 11450078). The authors gratefully acknowledge Mr. Y.Akasaka for his experimental cooperation. The authors gratefully acknowledge Yamaha motor Co. Ltd. for the supply of fuel injection system.

References

[1] F.Durst and M.Zaré 1975 *Proc. Laser Doppler anemometry symp.* (Copenhagen, Denmark) 403–429
[2] W.D.Bachalo, R.C.Rudoff, A.Brenda de la Rosa 1988 AIAA **88** 0236
[3] F.Durst, C.Tropea and T.H.Xu 1994 X.Shen and X.Sun eds. (International Academic Publishers, Beijing) 38–43
[4] T.Maeda, H.Morikita, K.Hishida and M.Maeda 1997 R.J.Adrian, D.F.G.Durao, M.V.Heitor, M.Maeda, J.H.Whitelaw eds. Developments in laser techniques and fluid mechanics (Springer Berlin Heidelberg New York) 268–287
[5] G.König, K.Anders and A.Frohn 1986 J. Aerosol Sci. **17** 157–167
[6] A.R.Glover, S.M.Skippon and R.D.Boyle 1995 Appl. Opt. **34** 8409–8421
[7] S.M.Skippon and Y.Tagaki 1996 Advances in Engine Combustion and Flow Diagnostics. (The Society for Automotive Engineers, Washington, DC) 183–198
[8] M.Maeda, T.Kawaguchi and K.Hishida 2000 Meas. Sci. Technol. **11** L13–L18
[9] T.Kawaguchi, Y.Akasaka and M.Maeda 2002 Meas. Sci. Technol. **13** 308–316
[10] M.Maeda, Y.Akasaka and T.Kawaguchi 2002 Exp. Fld. **33** 125–134
[11] T.Kobayashi, T.Kawaguchi and M.Maeda 2002 Laser Techniques for Fluid Mechanics R.J.Adrian, D.F.G.Durao, M.V.Heitor, M.Maeda, C.Tropea, J.H.Whitlaw eds. (Springer Berlin Heidelberg New York) 209–220
[12] H.C.Van de Hulst and R.T.Wang 1991 Appl. Opt. **30** 4755–4763
[13] K.Kobashi, K.Hishida and M.Maeda 1990 Application of Laser Techniques to Fluid Mechanics R.J.Adrian, D.F.G.Durao, M.V.Heitor, M.Maeda, J.H.Whitlaw eds. (Springer Berlin Heidelberg New York) 268–287
[14] M.Maeda, N.Sanai, K.Kobashi and K.Hishida 1988 Proc. 4th International Symp. on Appl. of Laser Anemometry to Fluid Mech. Lisbon, July 11–14